Aerospace Science and Technology 92 (2019) 489–500

Contents lists available at ScienceDirect

Aerospace Science and Technology

www.elsevier.com/locate/aescte

A novel three-axis attitude stabilization method using in-plane internal mass-shifting

Liang He [a], Xiaoqian Chen [b,*], Krishna Dev Kumar [c], Tao Sheng [a], Chengfei Yue [d]

[a] College of Aerospace Science and Engineering, National University of Defense Technology, Changsha, 410073, China
[b] National Innovation Institute of Defense Technology, Beijing, 100081, China
[c] Department of Aerospace Engineering, Ryerson University, 350 Victoria St., Toronto, Ontario, M5B2K3, Canada
[d] Department of Electrical and Computer Engineering, National University of Singapore, 117583, Singapore

ARTICLE INFO

Article history:
Received 28 August 2018
Received in revised form 28 April 2019
Accepted 11 June 2019
Available online 14 June 2019

Keywords:
Spacecraft
Attitude stabilization
Mass-shifting
Aerodynamic
Angular momentum
Sliding mode

ABSTRACT

This paper investigates the feasibility of using four movable masses distributed in a plane to realize three-axis attitude stabilization. With the proposed distribution and moving the paired masses in the same or opposite direction simultaneously, aerodynamic torque or internal momentum exchange torque is acted on the spacecraft. Then the spacecraft is gradually stabilized under a three-phase control strategy. Each of the three control phases is designed based on optimal control, nonlinear and sliding mode control, respectively. The stability of the proposed controller is given. Furthermore, numerical simulation matches the analytical results presented in this paper. Results show that three-axis attitude stabilization is possible using only in-plane movable masses which weigh less than 10 percent of spacecraft mass. Finally, the proposed control system can be a viable alternative for three-axis attitude stabilization of spacecraft orbiting in low Earth orbit.

1. Introduction

Most space applications need special orientation, thus an attitude control system is essential for these spacecrafts. Typical attitude control systems for orbiting spacecraft are mainly based on the use of three types of actuators: mass expulsion devices [1], angular momentum exchange devices [2], and environmental interacting devices. For environmental interacting devices, the most commonly used device is magnetic torquer [3–5]. And the use of aerodynamic drag [6,7], gravity gradient torque [8] and solar radiation pressure [9,10] to control spacecraft has also been investigated. For low Earth orbit (LEO), aerodynamic drag is typically the main force act on the spacecraft, but in most researches, it was treated as disturbances [11]. While in this paper, aerodynamic drag is considered as the source of external control torque during the stabilization.

Existing works mainly focus on rigid spacecrafts [12,13]. However, complex spacecrafts have become increasingly common in the light of the diversity of mission requirements. Dynamics and control of a spacecraft considering movable parts have been extensively investigated [14]. The movable part can be a manipulator [15], a flexible solar panel [16], or a fuel tank [17], etc. Meanwhile, some efforts were made to use the control torque generated by internal mass-shifting. In general, internal mass motion have three effects, one of which is that mass-shifting can change the relative position between center of mass (CM) and center of pressure (CP) which can generate aerodynamic torque. Atkins et al. [18] proposed a method to use internal moving mass actuator control for Mars entry guidance. Simone Chesi et al. [19] proposed an adaptive nonlinear attitude regulation control law for spacecraft using three movable masses with one reaction wheel or three magnetic torquers to achieve three-axis attitude stabilization. The second effect is that mass-shifting can change distribution of angular momentum in the body frame. In particular, Terry [20] proposed a rotational kinetic energy dissipation method using one shifting mass to convert tumbling motion into simple spin. Kumar and Anmin [21] investigated linear quadratic regulator (LQR) method to achieve desired spin stabilized attitude using one movable mass. The third effect is the change of the inertia tensor due to internal mass motion. Doroshin [22] investigated attitude dynamics and control of spacecraft in presence of inertia tensor change. The internal position of mass center is relocated, leading to change of force lever of the propulsion unit.

To the authors' best knowledge, there is not much emphasis in the literature on using movable masses only for three axis at-

* Corresponding author.
E-mail addresses: heliang09@nudt.edu.cn (L. He), chenxiaoqian@nudt.edu.cn (X. Chen), kdkumar@ryerson.ca (K.D. Kumar), shengtao-2002@163.com (T. Sheng), chengfei_yue@u.nus.edu (C. Yue).

https://doi.org/10.1016/j.ast.2019.06.019
1270-9638/

Nomenclature

CM	center of mass
CP	center of pressure
Param	Parameter
$\boldsymbol{h}_{CM}$	angular momentum about the CM of the spacecraft
$\boldsymbol{\omega}$	angular velocity with respect to inertial coordinate system
$\boldsymbol{r}_{CM}$	vector from origin to CM of spacecraft
$\boldsymbol{r}_{mpi}$	vector from origin to i-th movable mass
$\boldsymbol{I}_{CM}$	moment of inertia of main body with respect to CM of spacecraft
$\boldsymbol{I}$	moment of inertia of main body with respect to CM of main body
$\boldsymbol{r}_M$	radius of the orbit
μ_E	gravitational parameter of the Earth
$\boldsymbol{v}_o$	orbit linear velocity expressed in inertial coordinate system
$\boldsymbol{\omega}_{oi}^{o}$	orbit angular velocity expressed in orbital coordinate system
$\boldsymbol{f}_{d_i}$	aerodynamic force acting on the i-th face of the spacecraft
$\boldsymbol{v}_b$	linear velocity expressed in body-fixed coordinate system
$\boldsymbol{\tau}_{ext}$	total external torque acting on the spacecraft
$\boldsymbol{r}_{cpi}$	vector from the origin to the CP of i-th face
$\boldsymbol{\tau}_{cp}$	aerodynamic torque caused by misalignment of CM with CP of main body
$\boldsymbol{\tau}_m$	aerodynamic torque caused by misalignment of CM of movable masses with CM of main body
y_l, y_h	lower and upper limit of Y axis motion, $y_l y_h < 0$
z_l, z_h	lower and upper limit of Z axis motion, $z_l z_h < 0$
L_x, L_y, L_z	control function
sn, cn, dn	Jacobian elliptic functions

titude stabilization. This might be perhaps due to the system being underactuated [23], and controlling an underactuated system represents a challenging control problem. Except for the underactuated problem, the mass shifting system has its advantages compared with other actuators. Unlike momentum exchange devices like reaction wheels, it does not need to move after the control object is achieved. And compared with mass expulsion devices like thrusters, the system does not need propellant which will limit the life span of the control system. Just like Jianqing Li et al. have stated in [24], moving mass control has three desirable attributes compared with other control actuators (jet thruster or control moment gyroscope): light weight, simple structure and low power consumption. Moreover, moving mass control system only focus on the mass property, which means the mass could be a functional part of the spacecraft.

This paper aims to give a solution for three-axis stabilization using four movable masses. A spacecraft starts with an arbitrary rotational state, and its three-axis attitude is stabilized by controlling movable masses based on a three-phase control strategy. Firstly, an optimal control problem is proposed to control a control function to zero which corresponds to control the angular momentum component in the orbital frame. Secondly, the angular momentum of the spacecraft is assumed to be parallel to Y axis of orbital frame which is the control objective of the first phase. A nonlinear control law is designed to detumble the spacecraft into a simple Y-spin. Lastly, the spacecraft is assumed in simple Y spin state which is achieved by the second phase. After slowing down the spin rates, a sliding mode controller is used to design ideal torque based on the reduced dynamic system. The asymptotical stability property of proposed controller is proven by LaSalle's invariance principle. Since then, the three phases have formed a complete control system.

Compared with ref. [19], this paper only uses movable masses to complete three-axis stabilization while [19] uses three masses together with one reaction wheel or three magnetic torquers. If mass-shifting is used only to acquire aerodynamic torque, then the system is underactuated. That is the reason why it needs another actuator to make up, which makes the attributes of moving mass control stated in [24] lose luster. The major difference is that we take advantage of the internal momentum exchange torque which makes control problem of the underactuated system to be feasible. The main contributions of the paper are summarized as follows:

1) It is the first attempt to investigate the feasibility of a three-axis attitude control problem using movable masses only.

2) The angular momentum of the spacecraft is separated by defining a control function. An optimal control law is designed to find the optimum solution of masses' position so that the fastest way to align the angular momentum normal to the orbital plane is guaranteed.

3) We designed a control system with four movable masses in a plane. The motion of four masses is designed to combine two different effects of mass shifting together and isolate each other so that it can finally realize three-axis attitude stabilization control.

The rest of this paper is organized as follows. Section 2 presents system modeling of spacecraft, such as spacecraft dynamics including mass movement and spacecraft kinematics. Section 3 addresses the controller design procedures of three phases. The results of numerical simulations for all the phases are presented in Section 4. Finally, the concluding remarks of the present investigation are noted in Section 5.

2. Spacecraft model

2.1. Spacecraft dynamics

Assuming a spacecraft is composed of two parts (as shown in Fig. 1): rigid main body m_s and several movable masses m_{pi} (treated as a point mass). Three coordinate systems are considered (as shown in Fig. 2): an inertial coordinate system $O_E X_I Y_I Z_I$, an orbital coordinate system $O X_O Y_O Z_O$, and a body-fixed coordinate system $O X_b Y_b Z_b$. The inertial coordinate frame has its origin at the Earth center, and its X_I axis points to the first point of Aries, Z_I axis points to the North Pole, with its Y_I axis form a right-hand coordinate frame. The orbital coordinate system has its origin at the center of mass of the spacecraft, with the Z_O axis pointing to the nadir direction, the Y_O axis pointing to the direction of the orbit antinormal, and the X_O axis forming a right-hand coordinate frame. We assume the center of mass of the main body m_s lies at the origin of the body-fixed frame, with the axes being parallel to the principal axes of inertia.

According to the definition of angular momentum, the spacecraft angular momentum about the center of mass can be described by the following equation:

$$\boldsymbol{h}_{CM} = \boldsymbol{I}_{CM}\boldsymbol{\omega} + \sum_{i=1}^{n} m_{pi}\left(\boldsymbol{r}_{mpi} - \boldsymbol{r}_{CM}\right) \times \mathring{\boldsymbol{r}}_{mpi} \tag{1}$$

where $\boldsymbol{\omega} \in \boldsymbol{R}^3$ is the angular velocity of the body-fixed coordinate system with respect to the inertial coordinate system, $\boldsymbol{r}_{CM}$ is the

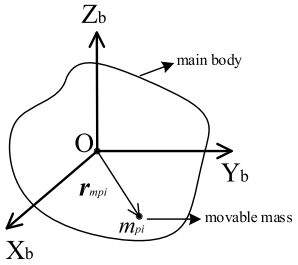

Fig. 1. Spacecraft containing movable mass.

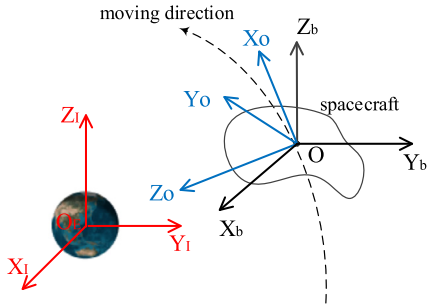

Fig. 2. Coordinate systems.

vector from origin to center of mass of spacecraft in $OX_bY_bZ_b$, $\boldsymbol{r}_{mpi}$ is the vector from origin to i-th movable mass and n is number of masses considered, $\overset{\circ}{\boldsymbol{r}}_{mpi}$ represents the change rate of the i-th movable mass's position in the body-fixed frame and $\boldsymbol{I}_{CM}$ is the moment of inertia of the main body with respect to center of mass of the spacecraft.

The form of $\boldsymbol{I}_{CM}$ can be obtained from [19]

$$\boldsymbol{I}_{CM} = \boldsymbol{I} - m_s \boldsymbol{r}_{CM}^{\times} \boldsymbol{r}_{CM}^{\times} - \sum_{i=1}^{n} m_{pi} \left(\boldsymbol{r}_{mpi} - \boldsymbol{r}_{CM}\right)^{\times} \left(\boldsymbol{r}_{mpi} - \boldsymbol{r}_{CM}\right)^{\times} \tag{2}$$

where $\boldsymbol{I}$ is the moment of inertia matrix of the main body with respect to the center of mass of the main body, $\boldsymbol{a}^{\times}$ is the skew-symmetric matrix which is defined by

$$\boldsymbol{a}^{\times} = \begin{bmatrix} 0 & -a_3 & a_2 \\ a_3 & 0 & -a_1 \\ -a_2 & a_1 & 0 \end{bmatrix} \tag{3}$$

where $\boldsymbol{a} = [a_1 \ a_2 \ a_3]^T$.

By the definition of the center of mass, we have

$$\boldsymbol{r}_{CM} = \sum_{i=1}^{n} \frac{m_{pi}}{M} \boldsymbol{r}_{mpi} \tag{4}$$

where $M = m_s + \sum_{i=1}^{n} m_{pi}$ is the mass of the spacecraft.

Using Euler's momentum equation, the equation of the given system can be written as:

$$\boldsymbol{I}\dot{\boldsymbol{\omega}} + \boldsymbol{\omega} \times \boldsymbol{I}\boldsymbol{\omega} + \frac{d\boldsymbol{n}}{dt} + \boldsymbol{\omega} \times \boldsymbol{n} = \boldsymbol{\tau}_{ext} \tag{5}$$

where $\boldsymbol{n} = \sum_{i=1}^{n} m_{pi} \boldsymbol{A}_i \overset{\circ}{\boldsymbol{r}}_{mpi} - \sum_{i=1}^{n} m_{pi} \boldsymbol{A}_i^2 \boldsymbol{\omega} - m_s \boldsymbol{B}^2 \boldsymbol{\omega}$, $\boldsymbol{A}_i = \left(\boldsymbol{r}_{mpi} - \sum_{i=1}^{n} \frac{m_{pi}}{M} \boldsymbol{r}_{mpi}\right)^{\times}$, $\boldsymbol{B} = \left(\sum_{i=1}^{n} \frac{m_{pi}}{M} \boldsymbol{r}_{mpi}\right)^{\times}$ and $\boldsymbol{\tau}_{ext}$ is the total external torque acting on the spacecraft.

In this paper, the following assumptions are made to simplify theoretical analysis or simulation:

Assumption 1. The spacecraft is orbiting in a circular orbit.

Assumption 2. Each face of the spacecraft is flat and regular, and projection of the origin on a face is at the center of the face.

Assumption 3. The principal moments of inertia of spacecraft main body satisfies: $I_y = \max\{ I_x \ I_y \ I_z \}$.

Assumption 4. In a control interval Δt, the mass can be set to any position along its rail and both acceleration and velocity of all masses are zero at the end of the interval.

According to Assumption 1, the linear velocity $\boldsymbol{v}_o$ and angular velocity $\boldsymbol{\omega}_{oi}^{o}$ of the orbit have constant magnitude and can be written in scalar components in the orbital coordinate system as

$$\boldsymbol{v}_o = \sqrt{\frac{\mu_E}{\boldsymbol{r}_M}} \begin{bmatrix} 1 \\ 0 \\ 0 \end{bmatrix}, \boldsymbol{\omega}_{oi}^{o} = \sqrt{\frac{\mu_E}{\boldsymbol{r}_M^3}} \begin{bmatrix} 0 \\ -1 \\ 0 \end{bmatrix} \tag{6}$$

where $\boldsymbol{r}_M$ is the radius of the orbit and μ_E is the gravitational parameter of the Earth.

In this paper, we assume the spacecraft orbits in LEO. The main environmental force acting on the spacecraft is typically aerodynamic drag, which can be specified by different face of the spacecraft. Aerodynamic force acting on the i-th face of the spacecraft can be expressed by the following equation:

$$\boldsymbol{f}_{d_i} = -\frac{1}{2} C_D \rho(h) \left\| \boldsymbol{v}_b \right\|^2 \left(\hat{\boldsymbol{n}}_i^T \hat{\boldsymbol{v}}_b \right) \hat{\boldsymbol{v}}_b S_i, i = 1, 2, \ldots, p \tag{7}$$

where C_D is the aerodynamic drag coefficient, S_i and $\hat{\boldsymbol{n}}_i$ are respectively the surface area and the outward normal direction of the i-th surface. The number of the spacecraft's surfaces is indicated by p, and the atmospheric density, $\rho(h)$, is a function of the altitude. The spacecraft velocity expressed in body coordinate system, denoted by $\boldsymbol{v}_b \in R^3$, is given by

$$\boldsymbol{v}_b = \boldsymbol{R}_{ob} \boldsymbol{v}_o \text{ and } \hat{\boldsymbol{v}}_b = \frac{\boldsymbol{v}_b}{\left\| \boldsymbol{v}_b \right\|} \tag{8}$$

where $\boldsymbol{R}_{ob}$ is the rotational matrix from the body-fixed frame to the orbital frame. Since aerodynamic force is the only concerned external force, consequently

$$\boldsymbol{f}_{ext} = \sum_{i=1}^{p} \boldsymbol{f}_{d_i} \delta_i \tag{9}$$

The function δ_i is used to consider only the surface that impact against the gas particles rather than the one that is shadowed. The value is determined by

$$\delta_i = \begin{cases} 0, & \text{shadowed} \\ 1, & \text{otherwise} \end{cases} \tag{10}$$

The total torque acting on the spacecraft is given by the sum of the aerodynamic torques as

$$\boldsymbol{\tau}_{ext} = \sum_{i=1}^{p} \left(\boldsymbol{r}_{cpi} - \boldsymbol{r}_{CM} \right) \times \boldsymbol{f}_{d_i} \delta_i \tag{11}$$

where vector $\boldsymbol{r}_{cpi} \in R^3$ represents the vector starting from the origin to the center of pressure of i-th face expressed in $OX_bY_bZ_b$.

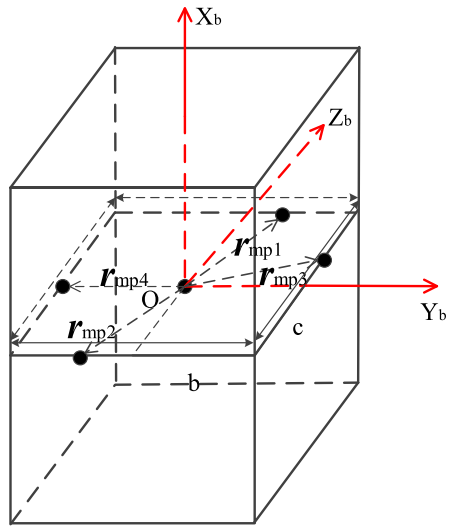

Fig. 3. Masses distribution.

By using the following definition

$$\boldsymbol{\tau}_{cp} = k_d \sum_{i=1}^{p} \left(\hat{\boldsymbol{n}}_i^T \hat{\boldsymbol{v}}_b \right) S_i \delta_i \boldsymbol{r}_{cpi}^{\times} \hat{\boldsymbol{v}}_b \tag{12}$$

$$\boldsymbol{\tau}_m = \frac{k_d}{M} \sum_{j=1}^{n} m_{pj} \sum_{i=1}^{p} \left(\hat{\boldsymbol{n}}_i^T \hat{\boldsymbol{v}}_b \right) S_i \delta_i \hat{\boldsymbol{v}}_b \times \boldsymbol{r}_{mpj} = \sum_{j=1}^{n} m_{pj} k_m \hat{\boldsymbol{v}}_b \times \boldsymbol{r}_{mpj} \tag{13}$$

where $k_d \triangleq -\frac{1}{2} C_D \rho \| \boldsymbol{v}_b \|^2$ and $k_m \triangleq \frac{k_d}{M} \sum_{i=1}^{p} \left(\hat{\boldsymbol{n}}_i^T \hat{\boldsymbol{v}}_b \right) S_i \delta_i$.

The equation of motion of the system described by Eq. (5) can be rewritten as:

$$\boldsymbol{I}\dot{\boldsymbol{\omega}} + \boldsymbol{\omega} \times \boldsymbol{I}\boldsymbol{\omega} + \frac{d\boldsymbol{n}}{dt} + \boldsymbol{\omega} \times \boldsymbol{n} = \boldsymbol{\tau}_{cp} + \boldsymbol{\tau}_{\boldsymbol{m}} \tag{14}$$

2.2. Spacecraft kinematics

Use unit quaternion $\boldsymbol{q} \in R^4$ to describe attitude of the spacecraft, the attitude kinematic equations are written as:

$$\dot{q}_0 = -\frac{1}{2} \bar{\boldsymbol{q}}^T \boldsymbol{\omega} \tag{15}$$

$$\dot{\bar{\boldsymbol{q}}} = \frac{1}{2} \left(q_0 I_{3\times 3} + \bar{\boldsymbol{q}}^{\times} \right) \omega = \boldsymbol{Q}\left(\boldsymbol{q}\right) \boldsymbol{\omega} \tag{16}$$

where the unit quaternion is a vector defined by $\boldsymbol{q} = \left[q_0 \ q_1 \ q_2 \ q_3 \right]^T = \left[q_0 \ \bar{\boldsymbol{q}} \right]$ satisfying $\bar{\boldsymbol{q}}^T \bar{\boldsymbol{q}} + q_0^2 = 1$. $\bar{\boldsymbol{q}} \in R^3$ is the vector part while q_0 is the scalar part and $\boldsymbol{Q}\left(\boldsymbol{q}\right) = \frac{1}{2}\left(q_0 I_{3\times 3} + \bar{\boldsymbol{q}}^{\times} \right)$.

Rotational matrix $\boldsymbol{R}\left(\boldsymbol{q}\right)$ between the orbital frame and the body-fixed frame can be described as follows:

$$\boldsymbol{R}\left(\boldsymbol{q}\right) = \left(q_0^2 - \bar{\boldsymbol{q}}^T \bar{\boldsymbol{q}} \right) I_{3\times 3} + 2\bar{\boldsymbol{q}}\bar{\boldsymbol{q}}^T - 2q_0 \bar{\boldsymbol{q}}^{\times} \tag{17}$$

Note that $\| \boldsymbol{R}\left(\boldsymbol{q}\right) \| = 1$.

The relative velocity $\boldsymbol{\omega}_e$ of the body-fixed frame with respect to the orbital frame is defined as

$$\boldsymbol{\omega}_e = \boldsymbol{\omega} - \boldsymbol{R}\boldsymbol{\omega}_{oi} \tag{18}$$

where $\boldsymbol{\omega}_{oi}$ is the orbit angular velocity with respect to inertial frame.

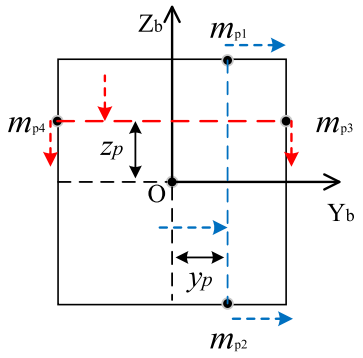

Fig. 4. Mass shifting in phase I.

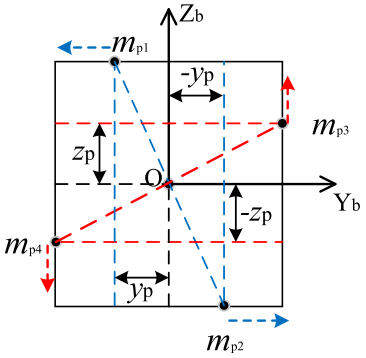

Fig. 5. Mass shifting in phase II.

3. Controller design

We consider two pairs of movable masses, p_1 and p_2, which can move parallel to Y_b and Z_b axes of the body-fixed coordinate system respectively (as shown in Fig. 3). Position vectors of all masses are defined as $\boldsymbol{r}_{mp1} = \left[0 \ y_1 \ c \right]^T$, $\boldsymbol{r}_{mp2} = \left[0 \ y_2 \ -c \right]^T$, $\boldsymbol{r}_{mp3} = \left[0 \ b \ z_3 \right]^T$, $\boldsymbol{r}_{mp4} = \left[0 \ -b \ z_4 \right]^T$, where b and c are constants depending on spacecraft's shape. All four masses are assumed to be equal: $m_{pi} = m_p, i = 1, \ldots, 4$.

Position of the movable mass is constrained by the size of the spacecraft and this constraint can be expressed in the following relation:

$$\boldsymbol{r}_{mpi} \in \{ \boldsymbol{r} | \boldsymbol{r} \in \boldsymbol{S} \}, i = 1, \ldots, n \tag{19}$$

where $\boldsymbol{S}$ is the set of all vectors inside the spacecraft.

This control system can make full use of two effects created by mass-shifting and can isolate this two effects. A three-phase control strategy is designed to accomplish three-axis attitude stabilization using movable masses. In phase I and phase III, aerodynamic torque is utilized, and while in phase II, we use the angular momentum redistribution effect. Each phase is explained as follows:

Phase I Angular momentum control

The objective of this phase is to align the angular momentum normal to the orbital plane. We assume $y_p = y_1 = y_2$ and $z_p = z_3 = z_4$ (as shown in Fig. 4). Then Eq. (13) can be written as:

$$\boldsymbol{\tau}_m = m_p k_m \hat{\boldsymbol{v}}_b \times \boldsymbol{r}_{mp} \tag{20}$$

where $\boldsymbol{r}_{mp} = \boldsymbol{r}_{mp1} + \boldsymbol{r}_{mp2} + \boldsymbol{r}_{mp3} + \boldsymbol{r}_{mp4} = \left[0 \ 2y_p \ 2z_p \right]^T$.

According to Assumption 2, we have:

$$\boldsymbol{\tau}_{cp} = \sum_{i=1}^{p} \boldsymbol{r}_{cpi}^{\times} \boldsymbol{f}_{di} \delta_i = 0 \tag{21}$$

Portions containing parameter $\boldsymbol{n}$ in Eq. (14) can be specified by

$$\begin{aligned}\frac{d\boldsymbol{n}}{dt}+\boldsymbol{\omega}\times\boldsymbol{n}=&\sum_{i=1}^{4}\left(m_p\dot{\boldsymbol{A}}_i+m_p\boldsymbol{A}_i\boldsymbol{\omega}^{\times}+m_p\boldsymbol{\omega}^{\times}\boldsymbol{A}_i\right)\mathring{\boldsymbol{r}}_{mpi}\\&-\left(\sum_{i=1}^{4}m_p\boldsymbol{A}_i^2+m_s\boldsymbol{B}^2\right)\dot{\boldsymbol{\omega}}+\sum_{i=1}^{4}m_p\boldsymbol{A}_i\mathring{\mathring{\boldsymbol{r}}}_{mpi}\\&-\left(\sum_{i=1}^{4}m_p\left(\dot{\boldsymbol{A}}_i\boldsymbol{A}_i+\boldsymbol{A}_i\dot{\boldsymbol{A}}_i\right)+m_s\left(\dot{\boldsymbol{B}}\boldsymbol{B}+\boldsymbol{B}\dot{\boldsymbol{B}}\right)\right)\boldsymbol{\omega}\\&-\boldsymbol{\omega}^{\times}\left(\sum_{i=1}^{4}m_p\boldsymbol{A}_i^2+m_s\boldsymbol{B}^2\right)\boldsymbol{\omega}\end{aligned}\tag{22}$$

where

$$\dot{\boldsymbol{A}}_i=\left(\frac{m_s+3m_p}{M}(\dot{\boldsymbol{r}}_{mpi}+\boldsymbol{\omega}\times\boldsymbol{r}_{mpi})-\sum_{j=1,j\neq i}^{4}\frac{m_p}{M}(\dot{\boldsymbol{r}}_{mpj}+\boldsymbol{\omega}\times\boldsymbol{r}_{mpj})\right)^{\times}.$$

Define $\tilde{\boldsymbol{I}}=\boldsymbol{I}-\left(\sum_{i=1}^{4}m_p\boldsymbol{A}_i^2+m_s\boldsymbol{B}^2\right)$, in which $-\left(\sum_{i=1}^{4}m_p\boldsymbol{A}_i^2+m_s\boldsymbol{B}^2\right)$ denotes the inertial tensor change caused by the movable masses. Substituting Eq. (22) into Eq. (14) yields

$$\tilde{\boldsymbol{I}}\dot{\boldsymbol{\omega}}+\boldsymbol{M}\left(\boldsymbol{r}_{mpi},\boldsymbol{\omega}\right)\boldsymbol{\omega}+\sum_{i=1}^{4}\boldsymbol{N}_i\left(\boldsymbol{r}_{mpi},\boldsymbol{\omega}\right)\mathring{\boldsymbol{r}}_{mpi}+\sum_{i=1}^{4}m_p\boldsymbol{A}_i\mathring{\mathring{\boldsymbol{r}}}_{mpi}=\boldsymbol{\tau}_m\tag{23}$$

where $\boldsymbol{M}\left(\boldsymbol{r}_{mpi},\boldsymbol{\omega}\right)=-\left(\tilde{\boldsymbol{I}}\boldsymbol{\omega}\right)^{\times}-\sum_{i=1}^{4}m_p\left(\dot{\boldsymbol{A}}_i\boldsymbol{A}_i+\boldsymbol{A}_i\dot{\boldsymbol{A}}_i\right)-m_s\left(\dot{\boldsymbol{B}}\boldsymbol{B}+\boldsymbol{B}\dot{\boldsymbol{B}}\right)+\boldsymbol{\omega}\times\sum_{i=1}^{4}m_p\boldsymbol{A}_i^2$, $\boldsymbol{N}_i\left(\boldsymbol{r}_{mpi},\boldsymbol{\omega}\right)=m_p\dot{\boldsymbol{A}}_i+m_p\boldsymbol{A}_i\boldsymbol{\omega}^{\times}+m_p\boldsymbol{\omega}^{\times}\boldsymbol{A}_i$.

Define a control function as:

$$L_z=\frac{1}{2}V\boldsymbol{h}_{Oz}^T\boldsymbol{h}_{Oz}\tag{24}$$

where V is a positive constant and $\boldsymbol{h}_{Oz}$ is the angular momentum of the whole spacecraft parallel to the Z_O axis of the orbital frame. It is obvious that L_z is positive definite for all $\boldsymbol{h}_{Oz}\neq 0$. $\boldsymbol{h}_{Oz}$ can be calculated by

$$\boldsymbol{h}_{Oz}=(\boldsymbol{h}\cdot\boldsymbol{k}_O)\,\boldsymbol{k}_O\tag{25}$$

where $\boldsymbol{k}_O$ is unit vector of Z_O axis of orbital frame expressed in body-fixed frame. Then rate of the control function L_z is

$$\dot{L}_z=V\boldsymbol{h}_{Oz}^T\dot{\boldsymbol{h}}_{Oz}\tag{26}$$

We define $L=\frac{1}{2}V\boldsymbol{h}_O^T\boldsymbol{h}_O$, $L_x=\frac{1}{2}V\boldsymbol{h}_{Ox}^T\boldsymbol{h}_{Ox}$ and $L_y=\frac{1}{2}V\boldsymbol{h}_{Oy}^T\boldsymbol{h}_{Oy}$ to express angular momentum in all axes.

Use the following control strategy to realize optimal control:

Step 1: Calculate current angular momentum of the spacecraft parallel to the Z_O axis of orbital frame $\boldsymbol{h}_{Oz}=\begin{bmatrix}h_x & h_y & h_z\end{bmatrix}^T$ and L_z.

Step 2: If $L_z=0$, then $\boldsymbol{r}_{mp}=\boldsymbol{0}$.

If $L_z\neq 0$, find optimal $\boldsymbol{r}_{mpi}, i=1,\ldots,4$ to minimize $\dot{L}_z$, which subject to Eq. (19).

In order to decrease $\|\boldsymbol{h}_{Oz}\|$ without affecting $\|\boldsymbol{h}_{Oy}\|$, following condition must be satisfied:

$$\boldsymbol{h}_{Oz}\cdot\boldsymbol{r}_{mp}=h_y y_p+h_z z_p=0\tag{27}$$

The preceding equation always have at least one solution. Eq. (19) can be expressed as $y_l\le y_p\le y_h$, $z_l\le z_p\le z_h$, where y_l, y_h, z_l, z_h is the lower and upper limit of Y_b and Z_b axes, respectively. Here, we assume $y_l<0, y_h>0$ and $z_l<0, z_h>0$. In summary, the optimization problem is stated as:

Find optimal $\{y_p, z_p\}$ to minimize cost function $J=\int\dot{L}_z dt=\int V\boldsymbol{h}_{Oz}^T\dot{\boldsymbol{h}}_{Oz}dt$, subjected to

$$\begin{cases}h_y y_p+h_z z_p=0\\ y_l\le y_p\le y_h, y_l<0, y_h>0\\ z_l\le z_p\le z_h, z_l<0, z_h>0\end{cases}\tag{28}$$

Substituting Eq. (28) into Eq. (20) yields:

$$\frac{d\boldsymbol{h}}{dt}=m_p k_m\hat{\boldsymbol{v}}_b\times\boldsymbol{r}_{mp}=2m_p k_m\hat{\boldsymbol{v}}_b\times\begin{bmatrix}0 & 1 & -\frac{h_y}{h_z}\end{bmatrix}^T y_p\tag{29}$$

Thus the optimal y_p is the maximum or minimum value that satisfies $y_l\le y_p\le y_h$ and $z_l\le -\frac{h_y}{h_z}y_p\le z_h, h_z\neq 0$.

Step 3: Return to Step 1.

Theorem 1. *With Assumption 2, if the optimal control given by Eq. (28) is applied to the system model Eq. (23), then the angular momentum of a spacecraft can be aligned normal to the orbital plane ($\boldsymbol{h}\parallel\boldsymbol{h}_{Oy}$ and $\|\boldsymbol{h}_{Ox}\|=\|\boldsymbol{h}_{Oz}\|=0$).*

Proof. Rate of change of the spacecraft angular momentum can be written as:

$$\dot{\boldsymbol{h}}+\boldsymbol{\omega}\times\boldsymbol{h}=\boldsymbol{\tau}_{CM}=\sum_{i=1}^{p}\boldsymbol{r}_{CM}\times\boldsymbol{f}_{d_i}\delta_i=\boldsymbol{r}_{CM}\times\boldsymbol{f}_{ext}=k_m m_p\hat{\boldsymbol{v}}_b\times\boldsymbol{r}_{mp}\tag{30}$$

Then rate of change of modulus of angular momentum can be expressed as:

$$\begin{aligned}&\boldsymbol{h}^T\left(\dot{\boldsymbol{h}}+\boldsymbol{\omega}\times\boldsymbol{h}\right)=\boldsymbol{h}^T\dot{\boldsymbol{h}}=k_m m_p\boldsymbol{h}^T\left(\hat{\boldsymbol{v}}_b\times\boldsymbol{r}_{mp}\right)\\&=k_m m_p\boldsymbol{h}_{Ox}^T\left(\hat{\boldsymbol{v}}_b\times\boldsymbol{r}_{mp}\right)+k_m m_p\boldsymbol{h}_{Oy}^T\left(\hat{\boldsymbol{v}}_b\times\boldsymbol{r}_{mp}\right)\\&+k_m m_p\boldsymbol{h}_{Oz}^T\left(\hat{\boldsymbol{v}}_b\times\boldsymbol{r}_{mp}\right)\end{aligned}\tag{31}$$

where the subscript "O" represents the orbital frame.

In general, aerodynamic torque can change the total angular momentum. Also it can be noted that it can only provide torque perpendicular to the relative velocity between spacecraft and local atmosphere. Since $\hat{\boldsymbol{v}}_b$ is parallel to orbital X_O axis, $\boldsymbol{h}_{Ox}\cdot\boldsymbol{\tau}_{CM}=0$. By setting

$$\boldsymbol{h}_{Oz}\cdot\boldsymbol{r}_{mp}=0\tag{32}$$

then

$$\left(\hat{\boldsymbol{v}}_b\times\boldsymbol{r}_{mp}\right)\times\boldsymbol{h}_{Oz}=\boldsymbol{r}_{mp}\left(\hat{\boldsymbol{v}}_b\cdot\boldsymbol{h}_{Oz}\right)-\hat{\boldsymbol{v}}_b\left(\boldsymbol{r}_{mp}\cdot\boldsymbol{h}_{Oz}\right)=0\tag{33}$$

Thus $\hat{\boldsymbol{v}}_b\times\boldsymbol{r}_{mp}=\gamma\boldsymbol{h}_{Oz}$ holds, where $\gamma\in R$. Then

$$\boldsymbol{h}_{Oy}\cdot\boldsymbol{\tau}_{CM}=0\tag{34}$$

which indicates aerodynamic torque will not change angular momentum in orbital Y_O axis.

Change rate of modulus of $\boldsymbol{h}_{Oz}$ is

$$\boldsymbol{h}_{Oz}^T\dot{\boldsymbol{h}}_{Oz}=\gamma k_m m_p\boldsymbol{h}_{Oz}^T\boldsymbol{h}_{Oz}\tag{35}$$

Suppose that $\boldsymbol{r}_1$ is a solution of Eq. (32), and $\hat{\boldsymbol{v}}_b\times\boldsymbol{r}_1=\gamma_1\boldsymbol{h}_{Oz}$. Then, $\boldsymbol{r}_2=-\boldsymbol{r}_1$ is also a solution of Eq. (32), and $\hat{\boldsymbol{v}}_b\times\boldsymbol{r}_2=-\gamma_1\boldsymbol{h}_{Oz}$. Thus there must be at least a solution for:

$$\boldsymbol{h}_{Oz}^T\dot{\boldsymbol{h}}_{Oz}\le 0\tag{36}$$

The rotational matrix from inertial frame to orbital frame is given by

$$\boldsymbol{R} = R_1\left(-\frac{\pi}{2}\right) R_3\left(\omega + \frac{\pi}{2}\right) R_1(\Theta) R_3(\Omega) \tag{37}$$

where $R_i(\alpha)$ is the rotational matrix about ith axis with rotational angle α, $\omega = \omega_0 + \omega_{oi}t$ is the argument of perigee, Ω is the right ascension of ascending node, Θ is the inclination, ω_{oi} is the orbit angular velocity. Here, for simplicity, we assume $\Omega = \Theta = 0$. Then Eq. (37) can be written as:

$$\boldsymbol{R} = \begin{bmatrix} -\sin\omega & \cos\omega & 0 \\ 0 & 0 & -1 \\ -\cos\omega & -\sin\omega & 0 \end{bmatrix} \tag{38}$$

Angular momentum in the orbital frame is expressed as:

$$\boldsymbol{h}_O = \boldsymbol{R}\boldsymbol{h}_I = \begin{bmatrix} -h_{ix}\sin\omega + h_{iy}\cos\omega \\ -h_{iz} \\ -h_{ix}\cos\omega - h_{iy}\sin\omega \end{bmatrix} \tag{39}$$

which indicates that the angular momentum in the orbital Y_O axis remains unchanged while angular momentum in the orbital X_O and Z_O axes are exchanging due to the orbital motion. If no external torque is applied in corresponding direction, $\boldsymbol{h}_{Ox}^T\boldsymbol{h}_{Ox} + \boldsymbol{h}_{Oz}^T\boldsymbol{h}_{Oz} = h_{ix}^2 + h_{iy}^2 = \text{constant}$. With the proposed control law, the aerodynamic torque will keep reducing the modulus of $\boldsymbol{h}_{Oz}$. In other words, $h_{ix}^2 + h_{iy}^2$ will be diminished. Thus, $\|\boldsymbol{h}_{Ox}\|$ and $\|\boldsymbol{h}_{Oz}\|$ will be decreased to zero while $\|\boldsymbol{h}_{Oy}\|$ remains unchanged. Thereby, Theorem 1 is proven.

Remark 1: The definition of control function given by Eq. (24) can be changed to $L_y = \frac{1}{2}V\boldsymbol{h}_{Oy}^T\boldsymbol{h}_{Oy}$. Thus, using similar optimal control strategy and setting $\boldsymbol{h}_{Oy}^T \cdot \boldsymbol{r}_{mp} = 0$, the angular momentum in the orbital Y_O axis can get to any desired value.

Phase II Detumbling control

The control objective of this phase is to transfer angular momentum of the spacecraft to the body-fixed Y_b axis. In other words, the aim is to let the spacecraft rotate only about its' Y_b axis. We set $y_p = y_1 = -y_2$ and $z_p = z_3 = -z_4$ (as shown in Fig. 5). Assume that the initial angular momentum of spacecraft is parallel to the Y_O axis of the orbital frame. Eq. (23) can be expressed in component form as:

$$I_x\dot{\omega}_x = (I_y - I_z)\omega_y\omega_z + \sum_{i=1}^{n}(z_i f_{yi} - y_i f_{zi}) + \tau_{mx} \tag{40a}$$

$$I_y\dot{\omega}_y = (I_z - I_x)\omega_z\omega_x + \sum_{i=1}^{n}(x_i f_{zi} - z_i f_{xi}) + \tau_{my} \tag{40b}$$

$$I_z\dot{\omega}_z = (I_x - I_y)\omega_x\omega_y + \sum_{i=1}^{n}(y_i f_{xi} - x_i f_{yi}) + \tau_{mz} \tag{40c}$$

where ω_x, ω_y, ω_z are the angular velocity components of the spacecraft with respect to the inertial frame and expressed in the body-fixed frame; I_x, I_y, I_z are the principal moments of inertia of spacecraft main body; f_{xi}, f_{yi}, f_{zi} are defined forces acting on the ith control mass expressed in component form as:

$$f_{xi} = \mu_i(\ddot{x}_i - 2\dot{y}_i\omega_z + 2\dot{z}_i\omega_y - y_i\dot{\omega}_z + z_i\dot{\omega}_y + y_i\omega_x\omega_y + z_i\omega_x\omega_z - x_i(\omega_y^2 + \omega_z^2)) \tag{41a}$$

$$f_{yi} = \mu_i(\ddot{y}_i - 2\dot{z}_i\omega_x + 2\dot{x}_i\omega_z - z_i\dot{\omega}_x + x_i\dot{\omega}_z + z_i\omega_y\omega_z + x_i\omega_x\omega_y - y_i(\omega_x^2 + \omega_z^2)) \tag{41b}$$

$$f_{zi} = \mu_i(\ddot{z}_i - 2\dot{x}_i\omega_y + 2\dot{y}_i\omega_x - x_i\dot{\omega}_y + y_i\dot{\omega}_x + x_i\omega_x\omega_z + y_i\omega_y\omega_z - z_i(\omega_x^2 + \omega_y^2)) \tag{41c}$$

where μ_i is the reduced mass defined by

$$\mu_i = \frac{m_{pi}(M - m_{pi})}{M} = \frac{m_p(m_s + 3m_p)}{M} \tag{42}$$

With the distribution of the four masses, aerodynamic torque is

$$\boldsymbol{\tau}_m = m_p k_m \hat{\boldsymbol{v}}_b \times \boldsymbol{r}_{mp} = \boldsymbol{0} \tag{43}$$

From Eq. (43), one can get that angular momentum conservation for the spacecraft (including movable masses) holds.

Forces acting on m_{p2} and m_{p4} can be specified as:

$$f_{x2} = -f_{x1},\ f_{y2} = -f_{y1},\ f_{z2} = -f_{z1} \tag{44}$$

$$f_{x4} = -f_{x3},\ f_{y4} = -f_{y3},\ f_{z4} = -f_{z3} \tag{45}$$

Substituting Eq. (43), Eq. (44) and Eq. (45) into Eq. (40), yields

$$I_x\dot{\omega}_x = (I_y - I_z)\omega_y\omega_z + 2cf_{y1} + 2z_p f_{y3} - 2y_p f_{z1} - 2bf_{z3} \tag{46a}$$

$$I_y\dot{\omega}_y = (I_z - I_x)\omega_z\omega_x - 2cf_{x1} - 2z_p f_{x3} \tag{46b}$$

$$I_z\dot{\omega}_z = (I_x - I_y)\omega_x\omega_y + 2y_p f_{x1} + 2bf_{x3} \tag{46c}$$

The preceding equation shows that forces acting on the masses have effect on angular velocities in all axes. But if the initial angular momentum of the spacecraft is not zero and the external forces acting on the spacecraft are null, the spacecraft possesses momentum after the masses stop moving based on the principle of conservation of angular momentum. It is to be noted that Eq. (46) containing nonholonomic constraint [25] if initial angular momentum is not zero, which fails Brockett's necessary condition [26] for the existence of smooth, or even continuous, feedback control law to asymptotically stabilize the system to the equilibrium point. While with the angular momentum transferring effect of mass-shifting, we can develop control laws using the masses to transfer the angular momentum of the spacecraft to a specific orientation in the body-fixed frame.

Forces acting on the masses are selected as:

$$f_{y1} = -\mu c_1\dot{y}_p - \mu\left(c_2 + \omega_x^2 + \omega_z^2\right)y_p \tag{47}$$

$$f_{z3} = -\mu c_3\dot{z}_p - \mu\left(c_4 + \omega_x^2 + \omega_y^2\right)z_p \tag{48}$$

where c_1, c_2, c_3, c_4 are constants.

If no motion is applied, we have

$$I_x\omega_x^2 + I_y\omega_y^2 + I_z\omega_z^2 = 2T = \text{constant} \tag{49}$$

$$I_x^2\omega_x^2 + I_y^2\omega_y^2 + I_z^2\omega_z^2 = \|\boldsymbol{h}\|^2 = \text{constant} \tag{50}$$

where T is rotational kinetic energy and $\boldsymbol{h}$ is the angular momentum of the spacecraft.

As analyzed in [20], motion of control masses can change the rotational kinetic energy T. According to Assumption 3, I_y is the maximum among three principle moments of inertia, so that spinning body will be in stable angular motion once spinning is established [27].

For $\|\boldsymbol{h}\|^2 < 2I_zT$, which means $\frac{\omega_x^2}{\omega_y^2} > \frac{I_y(I_y - I_z)}{I_x(I_z - I_x)}$. If using internal mass moving can decrease ω_x^2 and ω_z^2 and in turn increase ω_y^2, then $\|\boldsymbol{h}\|^2 < 2I_zT \Rightarrow \|\boldsymbol{h}\|^2 > 2I_zT$ will finally be reached.

Then for $\|\boldsymbol{h}\|^2 > 2I_zT$, considering the analytical solution of Eq. (46) with no force applied, angular rates may be expressed in terms of Jacobian elliptic functions [28]:

For $I_y > I_z > I_x$

$$\omega_x = \gamma cn[p(t - t_0)] \tag{51a}$$

$$\omega_y = \alpha dn\left[p\left(t-t_0\right)\right] \tag{51b}$$

$$\omega_z = \beta sn\left[p\left(t-t_0\right)\right] \tag{51c}$$

where $cn^2x = 1 - sn^2x$, $dn^2x = 1 - k^2sn^2x\,(0 \le k \le 1)$.

Amplitude α, β, γ and precession frequency p can be found in the literature:

$$\begin{cases} \alpha = \sqrt{\frac{\boldsymbol{h}^2 - 2I_xT}{I_y\left(I_y - I_x\right)}},\ p = \sqrt{\frac{\left(\boldsymbol{h}^2 - 2I_xT\right)\left(I_y - I_z\right)}{I_xI_yI_z}} \\ \beta = \sqrt{\frac{2I_yT - \boldsymbol{h}^2}{I_z\left(I_y - I_z\right)}},\ k = \sqrt{\frac{I_z - I_x}{I_y - I_z}\frac{2I_yT - \boldsymbol{h}^2}{\boldsymbol{h}^2 - 2I_xT}} \\ \gamma = -\sqrt{\frac{2I_yT - \boldsymbol{h}^2}{I_x\left(I_y - I_x\right)}},\ I_y > I_z > I_x \end{cases} \tag{52}$$

For $I_y > I_x > I_z$

$$\omega_x = \beta sn\left[p\left(t-t_0\right)\right] \tag{53a}$$

$$\omega_y = \alpha dn\left[p\left(t-t_0\right)\right] \tag{53b}$$

$$\omega_z = \gamma cn\left[p\left(t-t_0\right)\right] \tag{53c}$$

Amplitude α, β, γ and precession frequency p are:

$$\begin{cases} \alpha = \sqrt{\frac{\boldsymbol{h}^2 - 2I_zT}{I_y\left(I_y - I_z\right)}},\ p = \sqrt{\frac{\left(\boldsymbol{h}^2 - 2I_zT\right)\left(I_y - I_x\right)}{I_xI_yI_z}} \\ \beta = \sqrt{\frac{2I_yT - \boldsymbol{h}^2}{I_x\left(I_y - I_x\right)}},\ k = \sqrt{\frac{I_x - I_z}{I_y - I_x}\frac{2I_yT - \boldsymbol{h}^2}{\boldsymbol{h}^2 - 2I_zT}} \\ \gamma = -\sqrt{\frac{2I_yT - \boldsymbol{h}^2}{I_z\left(I_y - I_z\right)}},\ I_y > I_x > I_z \end{cases} \tag{54}$$

From Eq. (51) to Eq. (54), it can be seen that the difference for $I_y > I_z > I_x$ and $I_y > I_x > I_z$ is just x and z are exchanged. Without losing generality, we assume $I_y > I_z > I_x$ in the following analysis.

Theorem 2. *With Assumption 3, if forces acting on the masses given by Eq. (47) and Eq. (48) are applied to the system model Eq. (46), and control system constants are chosen as:*

$$c_1^2 < 4c_2, c_3^2 < 4c_4 \tag{55}$$

$$c_1 > 0, c_2 > 0, c_3 > 0, c_4 > 0 \tag{56}$$

then ω_x and ω_z will converge to zero.

Proof. Substituting Eq. (47) into Eq. (41b), yields:

$$\ddot{y}_p + c_1\dot{y}_p + c_2y_p - c\dot{\omega}_x + c\omega_y\omega_z = 0 \tag{57}$$

Substituting Eq. (48) into Eq. (41c), yields:

$$\ddot{z}_p + c_3\dot{z}_p + c_4z_p + b\dot{\omega}_x + b\omega_y\omega_z = 0 \tag{58}$$

General solution of Eq. (57) and Eq. (58) are determined by control system constants c_1, c_2, c_3 and c_4. Since the constants are chosen as (55) and (56), the general solution of y_p and z_p are in the form of:

$$y_p = A_1e^{-k_1t}\sin\left(\lambda_1t\right) + A_2e^{-k_1t}\cos\left(\lambda_1t\right) \tag{59}$$

$$z_p = A_3e^{-k_2t}\sin\left(\lambda_2t\right) + A_4e^{-k_2t}\cos\left(\lambda_2t\right) \tag{60}$$

where A_1, A_2, A_3, A_4 are constants, and k_1 and k_2 are positive constants. And $r = -k_1 \pm \lambda_1 i$ are conjugate complex roots of equation $r^2 + c_1r + c_2 = 0$, $r = -k_2 \pm \lambda_2 i$ are conjugate complex roots of equation $r^2 + c_3r + c_4 = 0$. From (59) and (60), we can conclude that y_p and z_p are oscillatory and converging to zero.

By definition $F_1 = -c\dot{\omega}_x + c\omega_y\omega_z$, $F_2 = b\dot{\omega}_x + b\omega_y\omega_z$, substituting Eq. (51) into F_1 and F_2 yields

$$F_1 = c\left(\alpha\beta + \gamma p\right)sn\left[p\left(t-t_0\right)\right]dn\left[p\left(t-t_0\right)\right] \tag{61}$$

$$F_2 = b\left(\alpha\beta - \gamma p\right)sn\left[p\left(t-t_0\right)\right]dn\left[p\left(t-t_0\right)\right] \tag{62}$$

Substituting Eq. (60) and Eq. (62) into Eq. (58), yields:

$$\begin{aligned} &b\left(\alpha\beta - \gamma p\right)sn\left[p\left(t-t_0\right)\right]dn\left[p\left(t-t_0\right)\right] \\ &= e^{-k_2t}\left(C_1\sin\left(\lambda_2t\right) + C_2\cos\left(\lambda_2t\right)\right) \end{aligned} \tag{63}$$

where C_1, C_2 are constants.

Both sides of Eq. (63) are oscillatory and the amplitude of the right side is decreasing in mass cycle and approaching zero, thus $\alpha\beta - \gamma p$ should also be decreased to zero. Note that α, p are always positive, β is nonnegative and γ is nonpositive and modulus of β and γ share the same tendency of changing, thus $\beta \to 0, \gamma \to 0$ which means ω_x and ω_z will converge to zero. Thereby, Theorem 2 is proven. □

Also note that at the end of control, we have

$$\boldsymbol{R}_{bo}\left(\boldsymbol{q}\right)\boldsymbol{h}_O = \boldsymbol{I}_{CM}\boldsymbol{\omega} \tag{64}$$

where $\boldsymbol{R}_{bo}$ is the rotational matrix between orbital frame and body-fixed frame and $\boldsymbol{h}_O$ is the angular momentum expressed in the orbital frame.

Eq. (64) can be expressed in component form as:

$$\left(2q_2q_3 - 2q_0q_1\right)h_{Oy} = 0 \tag{65a}$$

$$\left(2\left(q_0^2 + q_2^2\right) - 1\right)h_{Oy} = \left(I_y + 2\mu c^2\right)\Omega \tag{65b}$$

$$\left(2q_2q_3 - 2q_0q_1\right)h_{Oy} = 0 \tag{65c}$$

Since the above mentioned nonlinear control method does not actively control the value of Ω, then Eq. (65) have two possible solutions:

1) if the final angular velocity satisfies $\Omega = \frac{h_{Oy}}{I_y + 2\mu c^2}$, then $q_0^2 + q_2^2 = 1$ which means $q_1 = q_3 = 0$. In that case, $\varphi = 0$, $\psi = 0$, φ and ψ are roll and yaw angles respectively.

2) if the final angular velocity satisfies $\Omega = -\frac{h_{Oy}}{I_y + 2\mu c^2}$, then $q_1^2 + q_3^2 = 0$ which means $q_2 = q_0 = 0$. In that case, $\varphi = 0$, $\psi = \pi$ or $\varphi = \pi$, $\psi = 0$.

Phase III Single axis stabilization with bounded moving range

The objective of this phase is to finish the last step of realizing three-axis attitude stabilization of the spacecraft. Set $y_p = y_1 = y_2$ and $z_p = z_3 = z_4$ (as shown in Fig. 4). We assume that the spacecraft is only rotating by its Y_b axis of the body-fixed frame and Y_b axis of body-fixed frame is parallel to Y_O axis of the orbital frame (means $\boldsymbol{h} = \boldsymbol{h}_{Oy} = \boldsymbol{h}_{by}$). Note that, this assumption contains two possible situations: 1) $q_1 = q_3 = 0$, 2) $q_2 = q_0 = 0$. The second can be controlled to the first. Here we only discuss the first situation in detail. To simplify the control process, keep spacecraft rotate just in Y_b axis. And aerodynamic torque in Eq. (20) is rewritten as:

$$\boldsymbol{\tau}_m = m_pk_m\hat{\boldsymbol{v}}_b \times \boldsymbol{r}_{mp} = m_pk_m\begin{bmatrix} -2y_pv_{bz} & -2z_pv_{bx} & 2y_pv_{bx} \end{bmatrix}^T \tag{66}$$

where $\hat{\boldsymbol{v}}_b = \begin{bmatrix} v_{bx} & v_{by} & v_{bz} \end{bmatrix}^T$.

In order not to arouse rotation on X_b and Z_b axis, set $y_p \equiv 0$. Thus, with Assumption 4, a reduced dynamic and kinematic system is generated:

$$\left(I_y + 2\mu c^2 + 2\mu z_p^2\right)\dot{\omega}_2 = -2m_pk_mv_{bx}z_p \tag{67}$$

$$q_2 = \sin\frac{\theta}{2},\ q_0 = \cos\frac{\theta}{2} \tag{68}$$

$$\dot{\theta} = \omega_y \tag{69}$$

where θ is the pitch angle. It is readily to get $\hat{v}_b = \left[\cos\theta \;\; 0 \;\; \sin\theta\right]^T$, $k_m = \frac{1}{M}k_d\left(S_1\left|\cos\theta\right| + S_2\left|\sin\theta\right|\right)$. Substituting Eq. (69) into Eq. (67), yields:

$$\begin{aligned}\dot{\omega}_y = \ddot{\theta} &= -\frac{2m_p k_m v_{bx} z_p}{I_y{+}2\mu c^2 + 2\mu z_p^2} \\ &= -\frac{2m_p k_d \cos\theta z_p}{M\left(I_y{+}2\mu c^2 + 2\mu z_p^2\right)}\left(S_1\left|\cos\theta\right| + S_2\left|\sin\theta\right|\right) \\ &= k_\epsilon \cos\theta z_p\end{aligned} \tag{70}$$

where $k_\epsilon = -\frac{2m_p k_d\left(S_1\left|\cos\theta\right| + S_2\left|\sin\theta\right|\right)}{M\left(I_y{+}2\mu c^2 + 2\mu z_p^2\right)} > 0$.

Considering aerodynamic torque is in small magnitude, the first step is to slow down the spinning rate of the spacecraft to a small value ω_t, which is chosen according to the magnitude of control torque so that angular velocity can be controlled to zero during the stabilization. This process can be done by simple PD controller:

$$\tau_{my} = -k_D\left(\omega_y - \omega_t\right) \tag{71}$$

where k_D is a positive constant.

Then wait for $|\theta| = \theta_h$ and $\theta\dot{\theta} < 0$, and it is just a matter of time. Here θ_h is the threshold of starting stabilization and $0 < \theta_h < \pi/2$, $\dot{\theta}(0) = \omega_t$.

We choose SMC to develop control algorithm as:

$$z_{pi} = -\left(\eta\,\mathrm{sgn}\left(s\right) + k_1 k_2\theta + \left(k_1 + k_2\right)\dot{\theta}\right)/\left(k_\epsilon\cos\theta\right) \tag{72}$$

where $\eta, k_1, k_2 \in R$ are positive constants, $s = \dot{\theta} + k_1\theta$, k_1 satisfies $0 < k_1^2 < \frac{-2m_p k_d S_m \cos\theta_h z_{min}}{M(I_y{+}2\mu c^2{+}2\mu z_{max}^2)\theta_h}$, in which $z_{min} = \min\left\{|z_l|, |z_h|\right\}$, $z_{max} = \max\left\{|z_l|, |z_h|\right\}$, $S_m = \min\left\{S_1, S_2\right\}$. 'sgn' is the signum function.

Considering that the masses' position is bounded within the spacecraft, when $z_{pi} > z_h$ or $z_{pi} < z_l$, we modify the algorithm to:

$$z_p = \begin{cases} z_l & s > 0\ \&\ \left(z_{pi} > z_h \text{ or } z_{pi} < z_l\right) \\ z_h & s < 0\ \&\ \left(z_{pi} > z_h \text{ or } z_{pi} < z_l\right) \\ z_{pi} & z_l < z_{pi} < z_h \end{cases} \tag{73}$$

Lemma 1. *$\theta(t)$ and $\dot{\theta}(t)$ are smooth functions of time, $\dot{\theta}(t)$ is derivation of $\theta(t)$ with time. Initially $\theta(0)\dot{\theta}(0) < 0$, $|\theta(0)| = \theta_h < \pi/2$. Define $V = s^2 = \left(\dot{\theta} + k_1\theta\right)^2$ with positive constant k_1 satisfying $k_1|\theta(0)| > \left|\dot{\theta}(0)\right|$, if $\dot{V} \le 0$ and for all values of $s \neq 0$, $\dot{V} < 0$, then $|\theta(t)| < \theta_h$ and $\left|\dot{\theta}(t)\right| < k_1\theta_h$.*

Proof. Both $\theta(t)$ and $\dot{\theta}(t)$ are smooth functions, $s(t) = \dot{\theta}(t) + k_1\theta(t)$ is a smooth function.

Without losing generality, suppose $\theta(0) > 0$, then $\dot{\theta}(0) < 0$, $s(0) = \dot{\theta}(0) + k_1\theta(0) > 0$. Here, we prove Lemma 1 by contradiction.

Suppose that there exist a $|\theta(t_k)| \ge \theta_h$.

If $\theta(t_k) > 0$, there must be a moment t_j satisfies $\theta(t_j) = \theta(0)$ and $\dot{\theta}(t_j) \ge 0$. Then $\left|s(t_j)\right| = \left|\dot{\theta}(t_j) + k_1\theta(0)\right| > |s(0)|$, which is not in accordance with $\dot{V} \le 0$.

If $\theta(t_k) < 0$, there must be a moment t_j satisfy $\theta(t_j) = -\theta(0)$ and $\dot{\theta}(t_j) \le 0$. Then $\left|s(t_j)\right| = \left|\dot{\theta}(t_j) - k_1\theta(0)\right| > |s(0)|$, which is not in accordance with $\dot{V} \le 0$. As a result, $|\theta(t)| < \theta_h$.

Suppose that there exist a $\left|\dot{\theta}(t_k)\right| \ge k_1\theta_h$.

If $\dot{\theta}(t_k) > 0$, there must be a moment $t_j < t_k$ satisfies $\dot{\theta}(t_j) = 0$ and $\theta(t_j) < \theta(t_k)$, then $|s(t_k)| = \left|\dot{\theta}(t_k) + k_1\theta(t_k)\right| > \left|k_1\theta(t_j)\right| = \left|s(t_j)\right|$, which is not in accordance with $\dot{V} \le 0$.

If $\dot{\theta}(t_k) < 0$, $s(t_k) = \dot{\theta}(t_k) + k_1\theta(t_k) < 0$, then there must be a moment $t_j < t_k$ satisfies $\left|s(t_j)\right| = \left|\dot{\theta}(t_j) + k_1\theta(t_j)\right| = 0$, then $|s(t_k)| = \left|\dot{\theta}(t_k) + k_1\theta(t_k)\right| > 0 = \left|s(t_j)\right|$, which is not in accordance with $\dot{V} \le 0$. As a result, $\left|\dot{\theta}(t)\right| < k_1\theta_h$.

Thereby, Lemma 1 is proven. □

Theorem 3. *A sliding mode surface is defined as $s = \dot{\theta} + k_1\theta$, if the control algorithm is chosen as (73) and applied to the system model Eq. (70), initial condition includes $\theta(0)\dot{\theta}(0) < 0$, $|\theta(0)| = \theta_h < \pi/2$, $k_1|\theta(0)| > \left|\dot{\theta}(0)\right|$, then $s = 0$ is asymptotically stable.*

Proof. Define a candidate Lyapunov function as:

$$V = \frac{1}{2}s^T s \tag{74}$$

It is obvious that V is positive semi-definite.

For $z_l < z_{pi} < z_h$, differentiating V with time yields:

$$\begin{aligned}\dot{V} &= s^T\dot{s} \\ &= s^T\left(\ddot{\theta} + k_1\dot{\theta}\right) \\ &= s^T\left(-\left(\eta\,\mathrm{sgn}\left(s\right) + k_1k_2\theta + \left(k_1 + k_2\right)\dot{\theta}\right) + k_1\dot{\theta}\right) \\ &= -\eta\left|s\right| - k_2 s^2 \le 0\end{aligned} \tag{75}$$

For $z_{pi} > z_h$ or $z_{pi} < z_l$, we have:

$$\begin{aligned}\dot{V} &= s^T\dot{s} \\ &= s^T\left(\ddot{\theta} + k_1\dot{\theta}\right) \\ &= s^T\left(k_\epsilon\cos\theta z_p + k_1\dot{\theta}\right)\end{aligned} \tag{76}$$

If for all $t \ge 0$, we have $|\theta(t)| \le \theta_h$ and $\left|\dot{\theta}(t)\right| < k_1\theta_h$, then $\cos\theta > \cos\theta_h > 0$ holds. Since $0 < -\frac{2m_p k_d S_m}{M(I_y{+}2\mu c^2{+}2\mu z_{max}^2)} \le k_\epsilon \le -\frac{2\sqrt{2}m_p k_d S}{M(I_y{+}2\mu c^2)}$, in which $S = \max\left\{S_1, S_2\right\}$, we have:

for $s > 0$

$$\begin{aligned}\dot{V} &= s^T\left(k_\epsilon\cos\theta z_p + k_1\dot{\theta}\right) \\ &< -\frac{2m_p k_d S_m\cos\theta_h s}{M(I_y + 2\mu c^2 + 2\mu z_{max}^2)}\left(z_l + z_{min}\right) \\ &\le 0\end{aligned} \tag{77}$$

and for $s < 0$

$$\begin{aligned}\dot{V} &= s^T\left(k_\epsilon\cos\theta z_p + k_1\dot{\theta}\right) \\ &< -\frac{2m_p k_d S_m\cos\theta_h s}{M\left(I_y{+}2\mu c^2 + 2\mu z_{max}^2\right)}\left(z_h - z_{min}\right) \\ &\le 0\end{aligned} \tag{78}$$

Combined with Lemma 1, then $|\theta(t)| \le \theta_h$ and $\left|\dot{\theta}(t)\right| < k_1\theta_h$ are guaranteed. As a result, V is negative definite for all values of $s \neq 0$. According to LaSalle's invariance principle [29], $s = 0$ is asymptotically stable. This conclusion can also be given using Barbalat's Lemma [29]. Thereby, Theorem 3 is proven.

In order to restrain the chattering phenomenon, the saturated function sat(s) is adopted instead of sgn(s) in Eq. (72) as:

$$\mathrm{sat}\left(s\right) = \begin{cases} 1 & s > \Delta \\ ks & |s| \le \Delta, k = 1/\Delta \\ -1 & s < \Delta \end{cases} \tag{79}$$

where Δ is the boundary layer. Outside the boundary layer we use switch control, and inside the boundary layer we use linear feedback control.

If initially we have $q_2 = q_0 = 0$, then first we can decrease pitch to zero and then use masses along Y_b track to decrease roll and yaw to zero, the controller in this situation can be designed similar to phase III. Thus, we are not discussing this case in this paper.

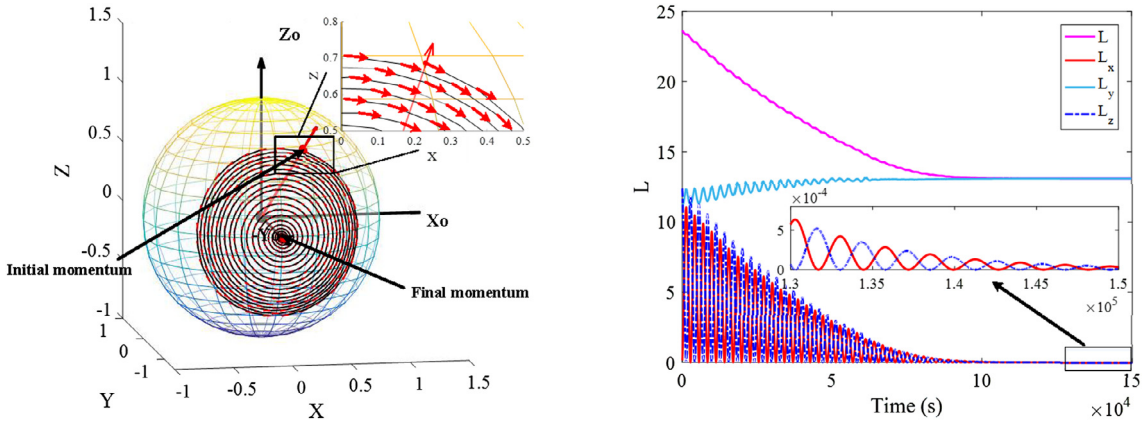

(a) Angular momentum vector change in orbital frame

(b) Change of control function L

Fig. 6. Angular momentum vector and control function change in orbital frame for Phase I. (For interpretation of the colors in the figure(s), the reader is referred to the web version of this article.)

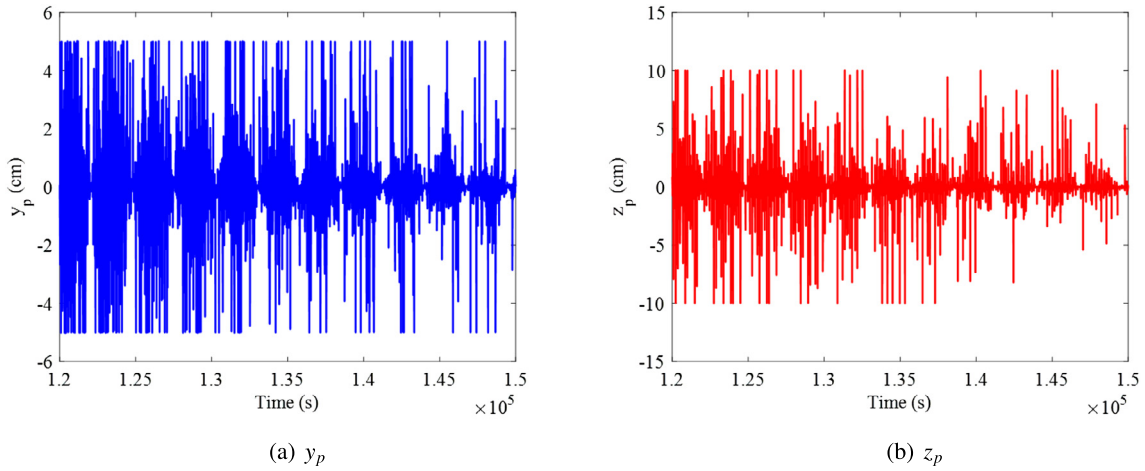

(a) y_p

(b) z_p

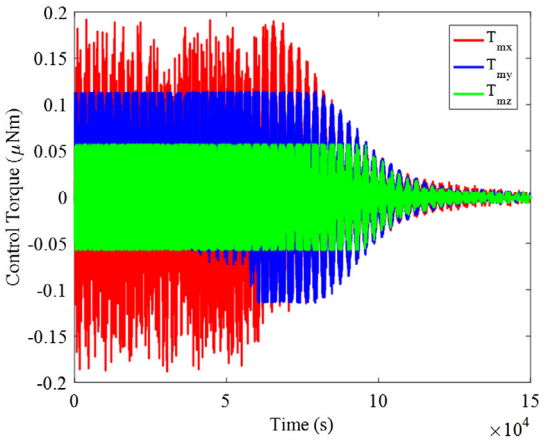

(c) Control torque

Fig. 7. Masses' position and control torque for Phase I. (For interpretation of the colors in the figure(s), the reader is referred to the web version of this article.)

Table 1
Orbital and system parameters.

Param	m_s kg	m_p kg	I_x kg · m^2	I_y kg · m^2	I_z kg · m^2	μ_E km^3 · s^{-2}	r_M km	i, Ω, ω, M rad
Value	7.6	0.2	0.035	0.091	0.070	398600	6728	0

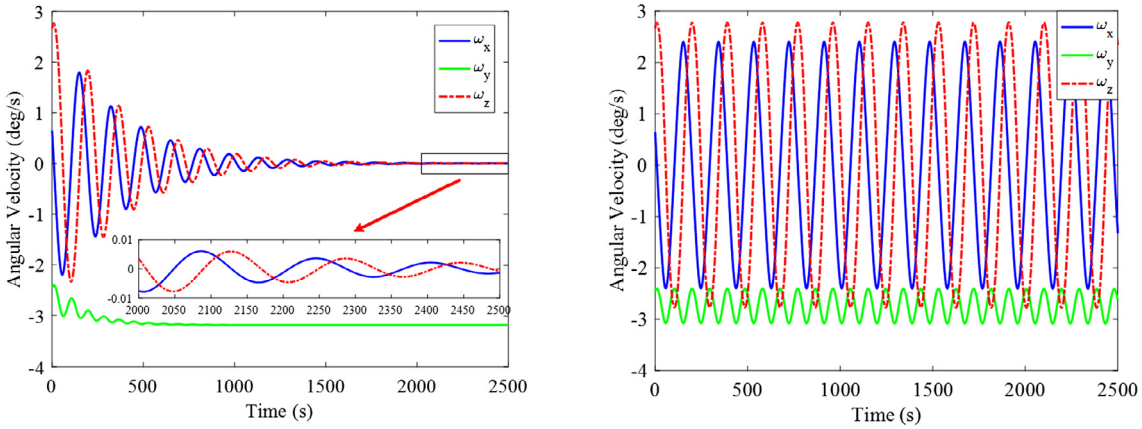

(a) Angular velocity with control (b) Angular velocity without control

Fig. 8. Angular velocity with and without control comparison for Phase II.

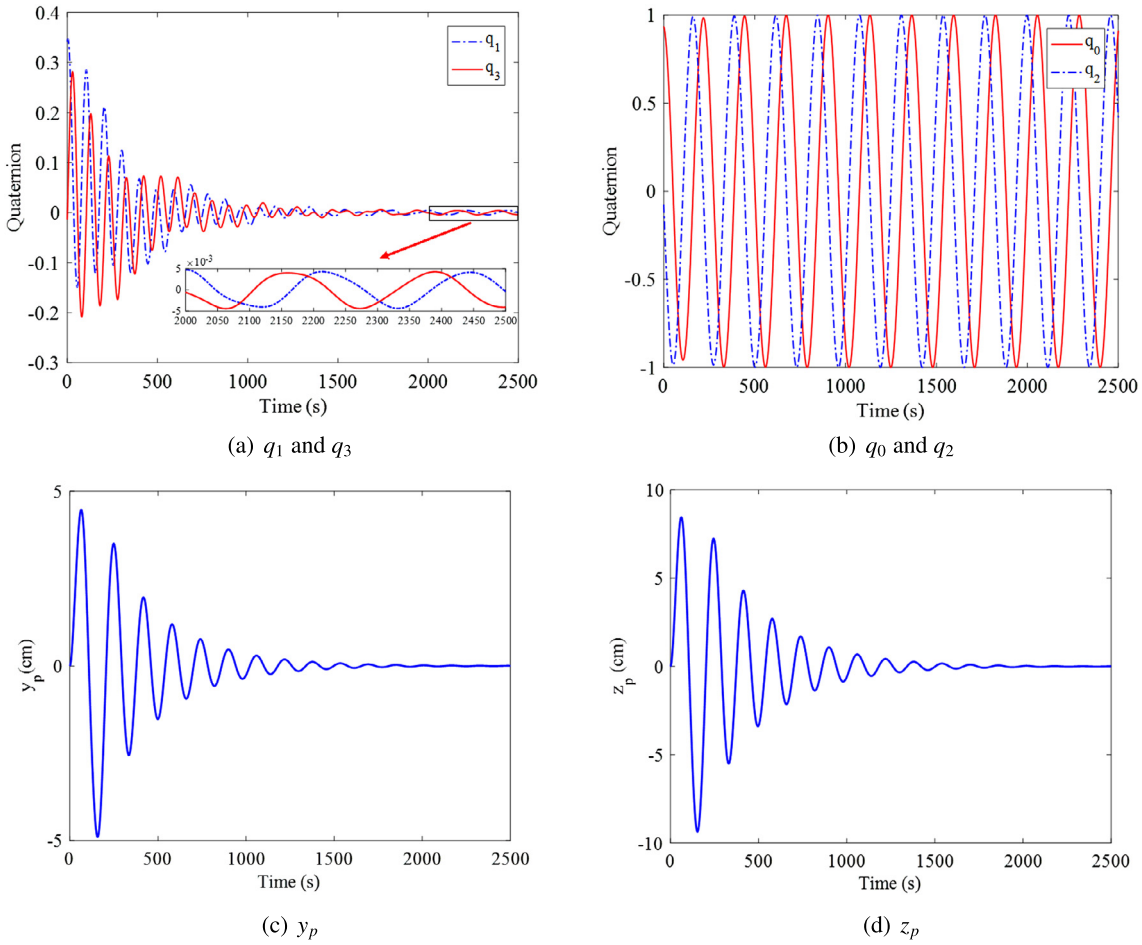

(a) q_1 and q_3 (b) q_0 and q_2

(c) y_p (d) z_p

Fig. 9. Quaternion response and masses' position change for Phase II.

4. Numerical simulations

To study the efficacy and performance of the proposed control strategy, several numerical simulations are carried out in MATLAB 2016. The numerical integrator used was the fourth-order Runge-Kutta with a fixed time step of $T_s = 1$ s. The system parameters and orbital parameters for the spacecraft (6U cubesat) used in the numerical simulations are shown in Table 1.

Area for each face is $S = \begin{bmatrix} 0.02 & 0.06 & 0.03 \end{bmatrix}$ m^2, corresponding to X_b, Y_b, Z_b axes, respectively. Movable masses' positions restrict to $-5 \leq y \leq 5$ (cm), $-10 \leq z \leq 10$ (cm). Atmospheric density is taken from 1976 U.S. standard atmospheric model.

The results of the numerical simulations using the proposed three-phase control strategy (control parameters are shown in Table 2 and initial conditions are shown in Table 3) are as follows:

Phase I: Angular momentum control

Fig. 6(a) shows the trajectory of spacecraft angular momentum vector in the orbital frame. The angular momentum vector is aligned to the Y_O axis in a spiral manner. It is to be noted (see Fig. 6(b)) that total angular momentum is decreased and the con-

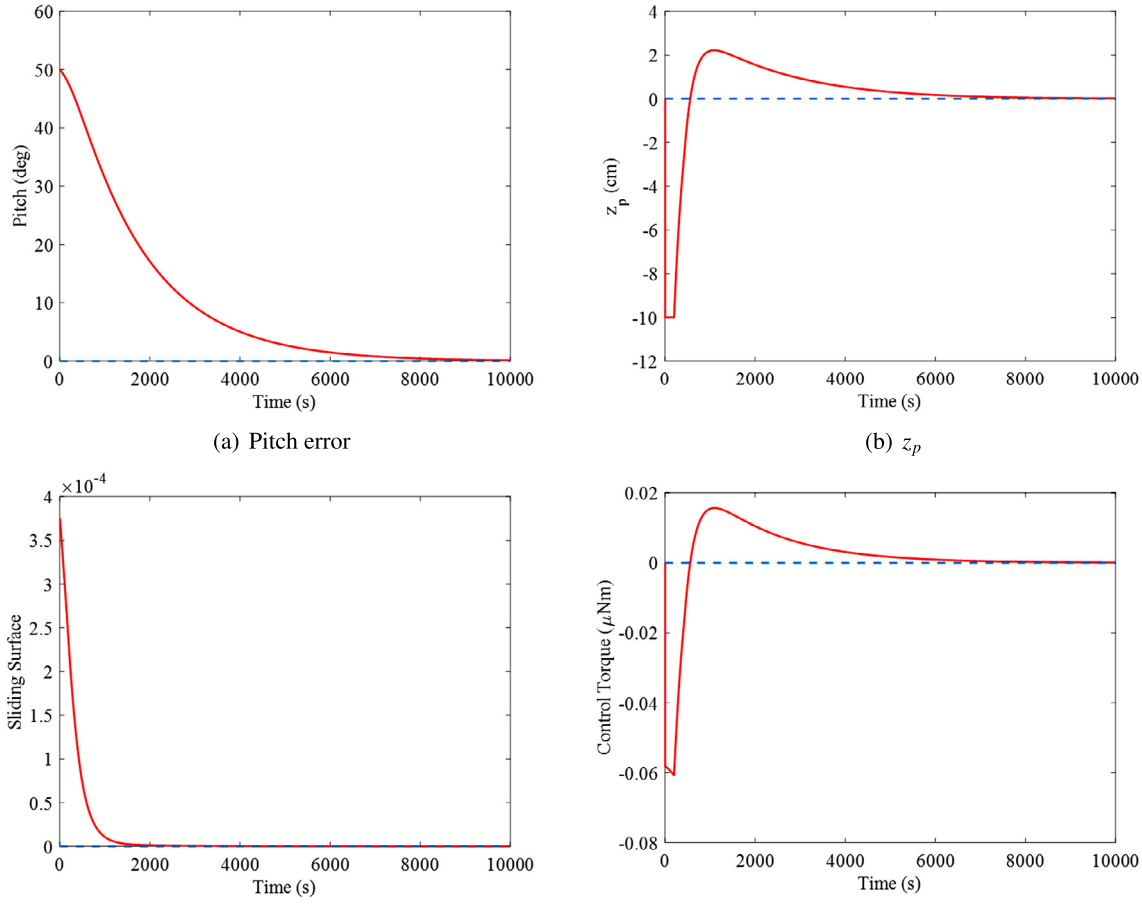

Fig. 10. Control results for Phase III.

Table 2
Control parameters.

Param	c_1	c_2	c_3	c_4	η	k_1	k_2
Value	0.05	0.001	0.05	0.001	10^{-7}	6.15×10^{-4}	3×10^{-3}

Table 3
Initial conditions for simulation scenarios.

Phase No.	q	ω_0 [deg/s]
Phase I	$[0.854 \quad -0.374 \quad 0.286 \quad -0.223]^T$	$[2.292 \quad -4.011 \quad 0.573]^T$
Phase II	$[0.936 \quad 0.342 \quad -0.076 \quad -0.014]^T$	$[0.644 \quad -2.458 \quad 2.666]^T$
Phase III	$[0.906 \quad 0 \quad 0.423 \quad 0]^T$	$[0 \quad -0.075 \quad 0]^T$

trol functions L_z converges to zero. The orbital motion leads to X_O and Z_O axes exchanging in quarter of orbital period which makes it possible to converge L_x to zero at the same time. Control function L_y oscillates in the beginning and the amplitude of oscillation decreases as seen in Fig. 6(b). The reason for L_y not being static is perhaps due to the consideration of the control delay in the numerical simulation as per Assumption 4. Fig. 7(a) and Fig. 7(b) show the position relocation of masses and they are limited to ± 5 cm and ± 10 cm. The control torque (Fig. 7(c)) generated by aerodynamic drag is within the magnitude of 0.2 μN m. After the desired angular momentum is achieved, the control is switched off; thereby, the masses are relocated to zero, leading to the next phase (phase II).

Phase II: Detumbling control

The total angular momentum expressed in the orbital frame is assumed to be $\boldsymbol{h}_O = [\,0 \;\; -0.0051 \;\; 0\,]^T$ (N m s), which is the value of angular momentum at the end of phase I. Fig. 8(b) shows the angular velocity responds without control. Referring to Fig. 8(a), the angular velocity about the X_b and Z_b axes converges to zero while the angular velocity about the Y_b axis converges to particular value (-3.18 deg/s). Meanwhile, Fig. 9(a) and Fig. 9(b) demonstrate that the quaternion error of q_1 and q_3 converge to zero and q_0 and q_2 are oscillating between ± 1. Fig. 9(c) and Fig. 9(d) show that all masses moving along the Y_b and Z_b axes are oscillating and the amplitudes of their oscillation are decreasing. The position y_p and z_p are bounded within ± 5 cm and ± 10 cm, respectively, and both converge to zero leading to the next phase (phase III).

Phase III: Single axis stabilization with bounded moving range

Fig. 10(a) shows that the pitch error converges to zero asymptotically. The position z_p (Fig. 10(b)) is bounded within ± 10 cm at the beginning and move towards zero at the end. Fig. 10(c) demonstrates the trajectory of the sliding surface, which converges to zero. Fig. 10(d) shows the control torque which is smaller than 0.08 μN m. Thus, three-axis attitude stabilization of spacecraft is achieved by following phase I, phase II and phase III based on in-plane mass-shifting.

5. Conclusions

An in-plane movable mass control system is proposed to achieve three-axis attitude stabilization. The proposed attitude control methodology is realized by a three-phase control strat-

egy. Firstly, an optimal control law is proposed to align the angular momentum normal to the orbital plane. Convergence property is proven for the proposed controller. Secondly, a nonlinear control law is adopted to detumble the spacecraft into a simple Y spin. Thirdly, a sliding mode control law is proposed to guarantee the asymptotically stabilization of pitch angle and its stability was proven by LaSalle's invariance principle. The performance of the proposed method is demonstrated through numerical simulations. In particular, we investigated a 6U cubesat on a circular orbit at 350 km of altitude. Simulation results show that by using those cascade phases, it is possible to realize three-axis attitude stabilization using four in-plane movable masses which weigh less than 10 percent of spacecraft. The proposed control system can be a viable alternative for three-axis attitude stabilization of spacecraft orbiting in LEO.

Extra work needs to be done for the proposed method putting into practice. Though aerodynamic torque is the major torque for LEO spacecraft, other torques like solar radiation and gravitation gradient may reduce the accuracy. In phase I, the control law is actually a feedback control law and is insensitive to disturbances. While in phase II and III, the proposed controllers cannot restrain disturbances. If this problem is considered, additional research is needed. While this paper focuses on solving the feasibility of a three-axis attitude control problem using movable masses, controllers considering disturbances will be discussed in our future work.

Declaration of Competing Interest

The authors declare there are no conflicts of interest regarding the publication of this paper.

Acknowledgements

This work was supported by the China Scholarship Council (Grant no. 201703170265), the National Natural Science Foundation of China (Grant no. 11725211) and the Scientific Research Project of National University of Defense Technology (Grant no. ZK 16-03-20).

References

[1] Y. Yoshimura, Optimal formation reconfiguration of satellites under attitude constraints using only thrusters, Aerosp. Sci. Technol. 77 (2018) 449–457, https://doi.org/10.1016/j.ast.2018.03.021.

[2] C. Yue, K.D. Kumar, Q. Shen, C.H. Goh, T.H. Lee, Attitude stabilization using two parallel single-gimbal control moment gyroscopes, J. Guid. Control Dyn. 42 (6) (2019) 1353–1364, https://doi.org/10.2514/1.G003445.

[3] K. Zhou, H. Huang, X. Wang, L. Sun, Magnetic attitude control for earth-pointing satellites in the presence of gravity gradient, Aerosp. Sci. Technol. 60 (2017) 115–123, https://doi.org/10.1016/j.ast.2016.11.003.

[4] A. Sofyalı, E.M. Jafarov, R. Wisniewski, Robust and global attitude stabilization of magnetically actuated spacecraft through sliding mode, Aerosp. Sci. Technol. 76 (2018) 91–104, https://doi.org/10.1016/j.ast.2018.01.022.

[5] D.S. Roldugin, P. Testani, Spin-stabilized satellite magnetic attitude control scheme without initial detumbling, Acta Astronaut. 94 (1) (2014) 446–454, https://doi.org/10.1016/j.actaastro.2013.01.011.

[6] S. Varma, K.D. Kumar, Multiple satellite formation flying using differential aerodynamic drag, J. Spacecr. Rockets 49 (2012) 325–336, https://doi.org/10.2514/1.52395.

[7] W.H. Steyn, H.W. Jordaan, An active attitude control system for a drag sail satellite, Acta Astronaut. 128 (2016) 313–321, https://doi.org/10.1016/j.actaastro.2016.07.039.

[8] S.A. Chee, J.R. Forbes, D.S. Bernstein, Gravity-gradient-stabilized spacecraft attitude estimation using rate-gyroscope measurements, in: 2016 American Control Conference, 2016, pp. 7067–7072.

[9] Y. Tsuda, G. Ono, T. Saiki, Y. Mimasu, N. Ogawa, F. Terui, Solar radiation pressure-assisted fuel-free sun tracking and its application to hayabusa2, J. Spacecr. Rockets 54 (6) (2017) 1284–1293, https://doi.org/10.2514/1.a33799.

[10] C.D. Petersen, F. Leve, M. Flynn, I. Kolmanovsky, Recovering linear controllability of an underactuated spacecraft by exploiting solar radiation pressure, J. Guid. Control Dyn. 39 (4) (2016) 826–837, https://doi.org/10.2514/1.g001446.

[11] C. Lu, C. Xiaoqian, S. Tao, The design of nonsingular terminal sliding-mode feedback controller based on minimum sliding-mode error, Proc. Inst. Mech. Eng., G J. Aerosp. Eng. 228 (9) (2013) 1540–1561, https://doi.org/10.1177/0954410013495492.

[12] B. Huo, Y. Xia, L. Yin, M. Fu, Fuzzy adaptive fault-tolerant output feedback attitude-tracking control of rigid spacecraft, IEEE Trans. Syst. Man Cybern. Syst. 47 (8) (2017) 1898–1908, https://doi.org/10.1109/TSMC.2016.2564918.

[13] E. Samiei, A.K. Sanyal, E.A. Butcher, Stabilization of rigid body attitude motion with time-delayed feedback, Aerosp. Sci. Technol. 68 (2017) 509–517, https://doi.org/10.1016/j.ast.2017.06.004.

[14] C. Grubin, Dynamics of a vehicle containing moving parts, J. Appl. Mech. 29 (3) (1962) 486–488, https://doi.org/10.1115/1.3640593.

[15] E. Arefinia, H.A. Talebi, A. Doustmohammadi, A robust adaptive model reference impedance control of a robotic manipulator with actuator saturation, IEEE Trans. Syst. Man Cybern. Syst. (2018) 1–12, https://doi.org/10.1109/TSMC.2017.2759148.

[16] W. He, S.S. Ge, Dynamic modeling and vibration control of a flexible satellite, IEEE Trans. Aerosp. Electron. Syst. 51 (2) (2015) 1422–1431, https://doi.org/10.1109/TAES.2014.130804.

[17] J.P.B. Vreeburg, Spacecraft maneuvers and slosh control, IEEE Control Syst. Mag. 25 (3) (2005) 12–16, https://doi.org/10.1109/MCS.2005.1432593.

[18] B.M. Atkins, E.M. Queen, Internal moving mass actuator control for Mars entry guidance, J. Spacecr. Rockets 52 (5) (2015) 1294–1310, https://doi.org/10.2514/1.a32970.

[19] C. Simone, G. Qi, R. Marcello, Aerodynamic three-axis attitude stabilization of a spacecraft by center-of-mass shifting, J. Guid. Control Dyn. 40 (7) (2017) 1613–1626, https://doi.org/10.2514/1.g002460.

[20] T.L. Edwards, M.H. Kaplan, Automatic spacecraft detumbling by internal mass motion, AIAA J. 12 (4) (1974) 496–502, https://doi.org/10.2514/3.49275.

[21] K.D. Kumar, A.-M. Zou, Attitude control of miniature satellites using movable masses, in: SpaceOps 2010 Conference, AIAA, 2010.

[22] A.V. Doroshin, Attitude dynamics of spacecraft with control by relocatable internal position of mass center, in: The International MultiConference of Engineers and Computer Scientists, vol. 1, 2017.

[23] A. Jain, Robot and Multibody Dynamics, Springer, 2011.

[24] J. Li, C. Gao, C. Li, W. Jing, A survey on moving mass control technology, Aerosp. Sci. Technol. 82–83 (2018) 594–606, https://doi.org/10.1016/j.ast.2018.09.033.

[25] J. Baillieul, P. Crouch, D. Zenkov, Nonholonomic Mechanics and Control, second edition, Springer, 2015.

[26] R.W. Brockett, Asymptotic stability and feedback stabilization, in: Differential Geometric Control Theory, 1983, pp. 181–191.

[27] M.J. Rycroft, R.F. Stengel, Spacecraft Dynamics and Control, Cambridge University Press, 1997.

[28] J.L. Synge, B.A. Griffith, Principles of Mechanics, McGraw-Hill, 1949.

[29] H.K. Khalil, Nonlinear Systems, Prentice Hall, 2002.